Journal of Solid State Chemistry 321 (2023) 123932

Contents lists available at ScienceDirect

Journal of Solid State Chemistry

journal homepage: www.elsevier.com/locate/jssc

Locating anionic hydrogen in $Ba_3(Yb,Lu)_2O_5H_2$: A combined approach of X-ray diffraction, crystal chemistry, and DFT calculations

Tiglet Besara [a,b,*], Daniel C. Ramirez [b], Jifeng Sun [c], Nathaniel W. Falb [b], Wangwei Lan [b,d], Jeffrey B. Whalen [b], David J. Singh [c], Theo Siegrist [b,e]

[a] Department of Physics, Astronomy, and Materials Science, Missouri State University, Springfield, MO, 65897, USA
[b] National High Magnetic Field Laboratory, Florida State University, Tallahassee, FL, 32310, USA
[c] Department of Physics and Astronomy, University of Missouri-Columbia, Columbia, MO, 65211, USA
[d] Department of Physics, Florida State University, Tallahassee, FL, 32306, USA
[e] Department of Chemical and Biomedical Engineering, FAMU-FSU College of Engineering, Florida State University, Tallahassee, FL, 32310, USA

A B S T R A C T

By a combination of x-ray diffraction, structural chemistry, and DFT calculations, the presence and location of anionic hydrogen in the two new, layered lanthanide oxyhydrides, $Ba_3Ln_2O_5H_2$ (Ln = Yb, Lu) is inferred. Single crystals of the compounds have been synthesized from a molten barium flux with the addition of small amounts of BaH_2. These phases crystallize in space group $I4/mmm$ (#139, $Z = 2$) with lattice parameters $a = 4.3336(2)$ Å and $c = 22.7197(6)$ Å, and $a = 4.3291(1)$ Å and $c = 22.597(1)$ Å, respectively. The $Ba_3Ln_2O_5H_2$ phases comprise two different structural moieties: a perovskite double layer of stoichiometry $Ba_2Ln_2O_5H^-$ formed by corner-connected LnO_5 tetragonal bi-pyramids with a terminating hydrogen anion, and a puckered rocksalt-type $(BaH)^+$ layer that is stretched along the c-axis. DFT calculations were used to arrive at hydrogen positions that minimize energy and are consistent with structural chemistry principles. Furthermore, the calculations show that the valence band edge is dominated by oxygen 2p orbitals with hydrogen 1s states admixed. The conduction band is formed by barium 5d-orbitals and Lu (Yb) 5d-orbitals. These are characteristics of materials with anionic H^-. These new phases are isostructural with the $Ba_3Ln_2O_5Cl_2$ (Ln = Gd–Lu) family of compounds with the chlorine atom in the same apical position as the hydrogen atom. Steric effects limit the size of the lanthanide ion for $Ba_3Ln_2O_5H_2$.

1. Introduction

Experimentally determining the presence of hydrogen in a crystal of an inorganic compound is – in principle – not hard: it can be done with both NMR and neutron diffraction. In the latter technique, the ^1H nucleus is a strong scatterer for neutrons, unlike in x-ray diffraction, making it easier to detect hydrogen in compounds and also determine their atomic positions. However, the inelastic scattering will be very high for hydrogen nuclei, so that samples are often deuterated to reduce the inelastic scattering background. In the former technique, one can perform solid-state ^1H NMR using two identical holders: one with and one without a sample. If there is a difference in spectrum, the presence of hydrogen in the sample is confirmed (and does not stem from sample holders, insulation around wires, etc.). The drawback to both techniques is the need for a relatively large amount of sample (on the order of several milligrams), more so for neutron diffraction than for solid state NMR. In a structure where the hydrogen atoms occupy a distinct Wyckoff position, their location can be determined by combining different methods and solid state chemistry principles.

In this manuscript we show that one can determine the presence of hydrogen in inorganic compounds by means of a combination of experimental techniques. Starting with x-ray diffraction and its subsequent structure analysis; a technique especially feasible if one does not have large amounts of sample where only one sub-millimeter crystal is needed. By carefully analyzing the results from a high-quality x-ray diffraction collection and applying fundamental crystal chemical principles, bond valence sums obtained from the experimentally determined structure, comparisons to isostructural compounds, and guidance by DFT electronic structure calculations, we show unambiguously the presence and the location of hydrogen atoms in two new oxyhydrides: $Ba_3Ln_2O_5H_2$ (Ln = Yb, Lu). We stress that this analysis works best if the hydrogen is on a distinct crystallographic position so that it is obvious that without the presence of a hydrogen anion, local electroneutrality is violated.

The field of multi-anion materials – typically where one of the anions is oxygen – is a rich area for functional materials with an incredibly wide range of compounds and applications. The field broadly encompasses oxypnictides, oxychalcogenides, oxyhalides, and oxyhydrides, and several review articles covering various compounds and topics can be found [1–9]. Of these, oxyhydrides is the group that has attracted most attention recently [5,6,10–16]. It is also the smallest group: Kageyama

* Corresponding author. Department of Physics, Astronomy, and Materials Science, Missouri State University, Springfield, MO, 65897, USA.
E-mail address: tigletbesara@missouristate.edu (T. Besara).

https://doi.org/10.1016/j.jssc.2023.123932
Received 14 September 2022; Received in revised form 17 February 2023; Accepted 18 February 2023
Available online 20 February 2023

et al. found in 2018 less than 50 oxyhydrides in the Inorganic Crystal Structure Database, compared to, e.g., over 300 oxypnictides (second smallest group) [6].

Oxyhydrides contain hydrogen as a distinct anion, the hydride H^-, in addition to the oxygen anion O^{2-}, unlike hydroxides which have the hydrogen closely bound to the oxygen to form $(OH)^-$ anions. The hydride anion has properties that make hydride-containing mixed-anions systems interesting and fascinating to study: it is flexible in size and can therefore adapt itself to different local environments; it can bond via covalent, ionic, and metallic bonding depending on the electronegativity of the bonding element; and it lacks *p* orbitals in its valence shell [6]. The hydride anion is expected to occupy a space similar to fluorine [17] and chlorine, and potentially isostructural phases related to fluorides and chlorides may exist.

The early oxyhydrides, LaOH in 1982 [18], and Ba_3AlO_4H and $Ba_{21}X_2O_5H_{22-24}$ (X = Ge, Si, Ga, In, Tl) in 1998 [19,20], were grown in a hydrogen atmosphere. Already in 1991, however, Schwarz reported flux growth of Ln_2LiHO_3 (Ln = rare earth metals) [21] using the alkali halide flux LiCl. This was, however, largely ignored. In 2002, the first oxyhydride compound was grown with a different method: growth of $LaSrCoO_4$ followed by reduction with CaH_2 to produce $LaSrCoO_3H_{0.7}$ [13]. It was not until recently that flux growth was revisited: $(La, Nd)_2LiHO_3$ were grown again with a LiCl flux [22–24], and La_2LiHO_3 [25] and $LaSrLiH_2O_2$ [26] were grown from a LiH self-flux.

The field has grown and many more oxyhydrides have been discovered with both transition metals and rare-earth metals: a few examples are layered perovskites $Ba_2(Sc,Y)HO_3$ [27,28] and Ln_2LiHO_3 [29]; layered strontium vanadium oxy-hydrides $SrVO_2H$, Sr_2VO_3H, and $Sr_3V_2O_5H_2$ [30,31]; Ruddlesden-Popper structures $LaSr_3NiRuO_4H_4$ [32,33], $LaSr_3CoRuO_4H_4$ [34], and $La_{2-x-y}Sr_{x+y}LiH_{1-x+y}O_{3-y}$ ($0 \leq x \leq 1$, $0 \leq y \leq 2$) [10]; perovskites $AETiO_{3-x}H_x$ (AE = alkaline earth metals) [35,36]; and fluorites LnOH [37–40].

In both the $La_{2-x-y}Sr_{x+y}LiH_{1-x+y}O_{3-y}$ structures [10] and the Ln_2LiHO_3 structures [29], the H^- ions occupy the equatorial sites of the Li^+ octahedra, while in the $LaSr_3(Ni,Co)RuO_4H_4$ structures, the H^- ions occupy the equatorial sites of the mixed Ni/Ru or Co/Ru octahedra [32–34]. In the strontium vanadium oxy-hydrides phases, on the other hand, the H^- ions occupy the apical sites of the V^{3+} octahedra [30,31]. In the $Ba_2(Sc,Y)HO_3$ structures, the H^- ions occupy one apical site in the (Sc,Y)-centered octahedra, although Ba_2ScHO_3 experiences partial anion ordering [27] while Ba_2YHO_3 has complete anion order [28]. The $AETiO_{3-x}H_x$ structures, on the other hand, show no preferential hydrogen positions but rather a random distribution of O^{2-} and H^- at the single anion site [35,36]. This is attributed to the absence of layering in the structure of these compounds [36]. In the LnOH phases, the lanthanide cation is 8-fold coordinated, forming edge-sharing cubes with four oxygen and four hydrogen anions [37,38]. For Ln = La–Nd, two types of cubes exist; ones where oxygen and hydrogen are each arranged in planes, and ones where oxygen and hydrogen are arranged tetrahedrally, while for Ln = Sm–Er, all anionic sites are disordered. In the case of Ba_3AlO_4H, AlO_4 tetrahedra are present, while the barium is coordinated by six oxygen and two hydrogen atoms [19]. Hydrogen is expected to be part of the Ba coordination polyhedron, while aluminum is bonded to oxygen exclusively. Specifically, H^- with its lower charge but similar size to O^{2-} preferentially coordinates the larger lower valence cation. It is also important to note that hydrogen has a much lower electronegativity than fluorine, a fact that explains its chemical flexibility and improved stability versus the oxyhydride. This further points to the fact that oxyhydrides are more difficult to form under excess O, such as in the formation of minerals.

We report on the self-flux growth of two new barium-lanthanide oxyhydride phases $Ba_3Yb_2O_5H_2$ and $Ba_3Lu_2O_5H_2$. Our continuous exploration of lanthanide oxide phases grown in metallic barium flux [41–43] resulted here in transparent crystals with apparent stoichiometry of $Ba_3Ln_2O_5$, but in very small yields. Based on the observed transparency of the crystals, charge balance is expected but is impossible to satisfy stoichiometrically for both phases since lutetium can only exist in the trivalent state, whereas ytterbium can exist in both divalent and trivalent states. Initial crystallographic studies confirmed the apparent stoichiometry, but the structures violated local electroneutrality. This led us to hypothesize that BaH_2, present as impurity in the barium metal used for the flux, may have contributed hydrogen to this phase, giving a charge compensated stoichiometry of $Ba_3Ln_2O_5H_2$ with anionic hydrogen on a distinct Wyckoff position. Adding BaH_2 to the flux immediately increased the yield and reproducibility of the crystal growth, confirming the hydrogen inclusion in this phase, and implying synthesis of a new oxyhydride phase. We proceeded to investigate the stability range of this structure by attempting synthesis with different lanthanides. The crystal structure is formed from perovskite double pyramidal layers $(Ba_2Ln_2O_5H)^-$ and $(BaH)^+$ layers, structurally identical to $Ba_3Ln_2O_5Cl_2$ [43], a $Ba_3Bi_2O_5I_2$-type structure [44]. To our knowledge, this is the first example of a lanthanide oxyhydride system with this structure-type. Of all existing oxyhalides in this structure-type, none contain lanthanides [45–52], except our previously reported $Ba_3Ln_2O_5Cl_2$ structures [43].

2. Material and methods

2.1. Synthesis

Single crystals of $Ba_3Ln_2O_5H_2$ (Ln = Yb, Lu) were prepared from a barium metal flux: 1 mmol of Ln_2O_3 powders, 0.25 mmol of BaO powder, and 0.5 mmol of BaH_2 powder were combined with 20 mmol of Ba metal pieces. The materials were loaded and sealed in stainless steel crucibles using a TIG welder under inert (argon) atmosphere in a glovebox. The steel crucibles were then sealed in quartz ampoules under vacuum. The samples were heated to 1000 °C in 10 h, solvated for 20 h, and slowly cooled to 820 °C in 200 h. At 820 °C – nearly 100 °C above the solidification temperature of barium (727 °C) to ensure that the flux remained liquid – the ampoules were removed from the furnace, inverted, and centrifuged to separate the flux from the crystals. The steel crucibles were cut open and the crystals were harvested under an inert atmosphere. The crystals are highly susceptible to ambient conditions, decomposing rapidly upon exposure to air and moisture. Sample integrity is maintained by handling and storing of the samples in an inert atmosphere.

2.2. X-ray diffraction and structural refinement

Single crystal X-ray diffraction data were collected using an Oxford-Diffraction Xcalibur-2 CCD diffractometer with graphite-monochromated Mo $K\alpha$ radiation. The crystals were mounted in cryoloops under Paratone-N oil and cooled to 180–200 K with an Oxford-Diffraction Cryojet using a cold N_2 gas stream. Data was collected using ω scans with 1° frame widths to a resolution of 0.4 Å, equivalent to $2\theta \approx 124°$ when possible. Indexing and absorption correction of reflections were carried out using the Rigaku Oxford Diffraction CrysAlisPro software [53]. Subsequent calculations used the X-ray structure refinement and analysis software CRYSTALS [54], employing Superflip [55] to solve the crystal structure. The data quality allowed for an unconstrained full matrix refinement against F^2 for the non-hydrogen atoms. The hydrogen atom was ultimately manually placed based on the structural analysis from the bond valence sum calculations and the theoretical calculations (see below) and was constrained to ride on the lanthanide atom. Anisotropic thermal displacement parameters were used for all non-hydrogen atoms while isotropic thermal displacement parameters were used for hydrogen. Crystallographic Information Files (CIFs) have been deposited with the Cambridge Crystallographic Data Centre (CCDC) ($Ba_3Yb_2O_5H_2$: CSD 2064988; $Ba_3Lu_2O_5H_2$: CSD 2064987) [56]. Elemental analysis via energy dispersive spectroscopy (EDS) was performed using a Zeiss 1540EsB scanning electron microscope equipped with an EDAX Apollo XPP SDD Detector.

2.3. Electronic structure calculations

Electronic structure calculations were performed using the linearized augmented plane-wave (LAPW) method [57] as implemented in the WIEN2K code [58]. We studied $Ba_3Lu_2O_5H_2$ as it has a full *f* shell, simplifying the calculation. The experimental lattice parameters were fixed but the atomic positions were relaxed with the standard Perdew, Burke and Ernzerhof (PBE) generalized gradient approximation (GGA) functional through total energy minimization [59]. The LAPW sphere radii were 2.4 bohr for Ba and Lu, 1.5 bohr for O and H. A basis set plane-wave cutoff parameter $R_{min}K_{max} = 7$ was used. This yields a high effective RK_{max} for the metal atoms due to their larger sphere radii compared with O and H. Additionally, local orbitals were used for the semicore states. A *k*-point grid of $8 \times 8 \times 8$ was used for the total energy calculations and a denser *k*-mesh of $17 \times 17 \times 17$ was employed for the calculations of density of states (DOS). Spin-orbit coupling was included for all the calculations except structure relaxations. An effective Coulomb potential $U = 8$ eV was used for the Lu *4f* states. This removes them from the vicinity of the band edges, and instead narrow spin orbit-split Lu *f* states occur at approximately 5 eV binding energy relative to the valence band maximum.

Calculations with hydrogen in different positions served to validate the optimal hydrogen location in the structure, and three structure models with different hydrogen positions were investigated. The energetically most favorable structure was subsequently used for electronic structure calculations.

3. Results and discussion

3.1. Synthesis

In addition to producing flat, plate-like $Ba_3(Yb,Lu)_2O_5H_2$ crystals, our synthesis method also produced needle-shaped single crystals of $Ba(Yb,Lu)_2O_4$, a family of compounds we reported on in 2004 and which were synthesized by adding Ln_2O_3 powders to Ba flux [42]. In the current reactions, $BaLn_2O_4$ crystals were produced in much greater yield than $Ba_3Ln_2O_5H_2$. In fact, $BaLn_2O_4$ crystals will always be produced in these reactions and always at greater yields than $Ba_3Ln_2O_5H_2$ since they do not rely on the impurity or addition of BaH_2. The yield ratio of $BaLn_2O_4$ to $Ba_3Ln_2O_5H_2$ was roughly 10:1 after we purposely added BaH_2.

The starting ratios were based on our previous trial growths of $Ba_3Ln_2O_5Cl_2$ [43]. We observed there that if we increased the amount of BaO, we obtained more $Ba_2Ln_2O_4$. Since the goal here is to produce $Ba_3Ln_2O_5H_2$ rather than $Ba_2Ln_2O_4$, we kept the amount of BaO small.

The single crystals of $Ba_3Ln_2O_5H_2$ were transparent, with layered, plate-like morphology (see Fig. 1), although thicker crystals tend to appear opaque. The crystals are expected to be colorless, however, mid gap states will produce colors, pink for Yb and red for Lu. This is consistent with the results of DFT calculations below, which show a band gap above the visible region, even with the PBE functional which typically underestimates band gaps.

The initial synthesis was conducted with Ln_2O_3 powders, BaO powder, and Ba metal pieces, and resulted in very small yields of the transparent flat crystals in addition to the greater yields of rods of $BaLn_2O_4$. EDS was performed on multiple crystals and showed the compounds having Ba:*Ln*:O molar ratios of 30:20:50 to within a few percent, thus confirming an apparent stoichiometry of $Ba_3Ln_2O_5$. The observed transparency further suggests charge-balanced compounds. While ytterbium can exist in a divalent oxidation state and thus render $Ba_3Yb_2O_5$ a possible compound, lutetium only exists in the trivalent oxidation state, making $Ba_3Lu_2O_5$ an impossible stoichiometry. Since the x-ray diffraction results (see below) tell us that the two compounds are isostructural, with commensurate lattice contraction when changing from Yb to Lu, it is reasonable to assume that $Ba_3Yb_2O_5$ did not form since $Ba_3Lu_2O_5$ cannot form. This led us to hypothesize that BaH_2, present in the barium metal used as flux, has contributed hydrogen to this phase, giving a charge-compensated stoichiometry of $Ba_3Ln_2O_5H_2$ (hydrogen cannot be detected with EDS) with Ln^{3+}. In fact, we have previously surmised that as-received Ba metal contains small amounts of hydrogen, likely from the reduction step in barium refining [60]. Deliberately adding BaH_2 to the flux in the current reactions immediately increased the yield, albeit still small, and the reproducibility of the crystal growth, confirming the hydrogen inclusion in this phase.

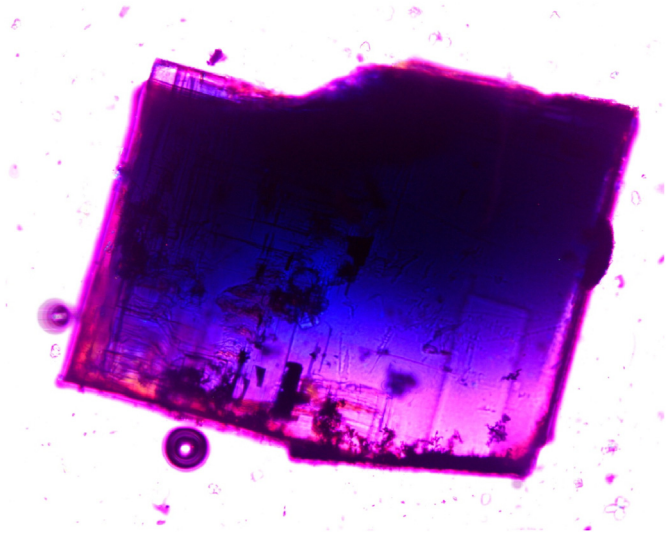

Fig. 1. Image of a crystal of $Ba_3Yb_2O_5H_2$ showing a tetragonal platelet habit (Nikon, differential interference contrast).

3.2. Structure and location of hydrogen

Initially, the crystal structure determinations converged rapidly and gave good residual for both structures even though it was obvious that $Ba_3Lu_2O_5$ would not be a viable structure due to the non-existent Lu^{2+} ion and the need for charge-balance. The apparent $Ba_3Ln_2O_5$ structure crystallized in space group *I4/mmm* and is illustrated in Fig. 2. Notice the "void" between the Ba1 layers. The lattice parameters are $a = 4.3336(2)$ Å and $c = 22.720(1)$ Å for $Ba_3Yb_2O_5$ and $a = 4.3291(1)$ Å and $c = 22.597(1)$ Å for $Ba_3Lu_2O_5$, following the expected lanthanide lattice contraction.

Employing the Bond Valence Sum (BVS) model [61,62] – a model relating bond lengths to oxidation states and based exclusively on experimentally obtained structural information and Pauling's rules [63] – we obtained BVSs for the apparent structures. The values are summarized in Table 1.

In the *Ln* = Lu case, we had to use the tabulated ideal bond length for Lu^{3+}– O since no Lu^{2+} values exist [64]. In the *Ln* = Yb case, when using the tabulated value for Yb^{2+}– O, we obtained a BVS of 3.0875 which clearly indicates that the Yb cation is trivalent or otherwise experience improbable overbonding if it is indeed divalent. Using the tabulated value for Yb^{3+}– O, we obtained 2.8936, just slightly under the ideal value of 3. The BVS for the two Ba atoms, on the other hand, are improbably underbonded. In the case of Ba1 – as can be seen by the "void" in Fig. 1 – this indicates that there is something missing in the vicinity of that atom. Ba2, on the other hand, is coordinated by twelve oxygen atoms and should not be that severely underbonded. In this case, a disorder of the O2 atom that is pancaked between two *Ln* atoms will remedy the Ba2 BVS. More on this further.

Upon further work on the refinement, difference Fourier maps indicated the presence of a small electron density between the barium layers. Refining an oxygen occupancy at this position, however, consistently gave approximately one to two electrons integrated. In addition to the results from the BVS calculations, local charge neutrality would require a negative charge in between the barium layers.

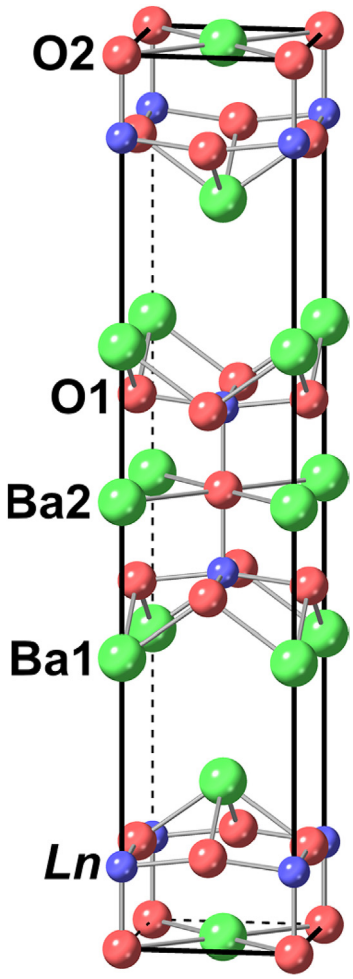

Fig. 2. Unit cell of the apparent structures $Ba_3Ln_2O_5$. *Ln* = blue atoms, Ba = green atoms, O = red atoms.

Table 1
Bond valence sums for the apparent structures $Ba_3Ln_2O_5$.

	$Ba_3Yb_2O_5$		$Ba_3Lu_2O_5$
	With Yb^{3+}	With Yb^{2+}	With Lu^{3+}
Ln	2.8936	3.0875	2.9945
Ba1	1.3042	1.3042	1.3042
Ba2	1.1837	1.1837	1.2253

With the collective knowledge that:

i) crystal transparency indicates charge-balanced structures,
ii) these two structures are isostructural with commensurate lanthanide lattice contraction,
iii) $Ba_3Lu_2O_5$ cannot exist since the Lu ion cannot be divalent, leading to the unlikeness of us synthesizing $Ba_3Yb_2O_5$,
iv) BVS analysis indicates trivalent lanthanide ions,
v) BVS analysis shows severely underbonded Ba atoms, requiring something else in the vicinity of the Ba atoms,
vi) local charge neutrality requires a negative charge in between the Ba layers,
vii) difference Fourier maps indicate electron density of one to two electrons between the layers, and
viii) addition of BaH_2 to the reactions improved the yield,

it is therefore experimentally shown that hydrogen indeed is included in these phases, rendering the charge-balanced structures $Ba_3Ln_2O_5H_2$ (*Ln* = Yb, Lu).

We did consider the possibility of these being so-called electrides [65,66]: ionic compounds where some electrons are not bound to an atom and could therefore be considered as "anions". In this case, the electrons would be located in between the barium ions. This case, however, is unlikely since electrides based on alkaline earth metals [67,68] (and alkali metals [69,70]) require high pressures.

Having confirmed that these structures must include hydrogen, the question then arises: where is the hydrogen located to satisfy local charge neutrality? Although the difference Fourier maps indicate a position, the presence of cations with large electron counts are expected to obscure the hydrogen position. Here, we can be guided by similarities with other structures (both oxyhydrides and oxyhalides), BVS analyses based on placing a hydrogen in distinct crystallographic sites in our x-ray diffraction-obtained structures, and ultimately DFT calculations.

The location of hydride ions in several different oxyhydrides was discussed in the Introduction. For many of the structures containing anion-coordinated octahedra, the H^- ions can occupy all or some of the equatorial sites of the octahedra [10,29,32–34], both apical sites [30,31], or one apical site [27,28]. And while some structures exhibit complete anion ordering, others show partial ordering, while some display random distribution of O^{2-} and H^- at a single anion site [35,36]. In one structure, Ln_2LiHO_3 [29], a Frenkel defect was considered: an equatorial hydride ion shifts to a position that was tetrahedrally coordinated. Of all these oxyhydrides, $Sr_3V_2O_5H_2$ has similar layering and structural motifs as our proposed compounds $Ba_3Ln_2O_5H_2$ but crystallizes in the orthorhombic space group *Immm* [30,31]. The H^- ion in $Sr_3V_2O_5H_2$ is located at both apical sites of the vanadium octahedron and in the same plane as Sr, forming planar SrH_2 layers.

We now look at other oxyhalides of similar composition to our compounds, and particularly alkaline earth metal oxyhalides: $AM_2O_5X_2$ (*A* = alkaline earth metals; *M* = transition, post-transition, or rare earth metals; and *X* = halides). Here, we find that $Ca_3Fe_2O_5Cl_2$ [47], $Sr_3Fe_2O_5Cl_2$ [46,47], $Sr_3Fe_2O_5Br_2$ [47], $Sr_3Co_2O_5Cl_2$ [49,50], $Ba_3In_2O_5F_2$ [45], $Ba_3In_2O_5Cl_2$ [71], $Ba_3In_2O_5Br_2$ [52], $Ba_3Tl_2O_5Cl_2$ [48], and $Ba_3Ln_2O_5Cl_2$ (*Ln* = Gd–Lu) [43] are all of the $Ba_3Bi_2O_5I_2$-type structure [44]. They all have the halide ion in one of the apical sites of the *M* octahedra while the other apical position is taken by an O^{2-} ion shared between two octahedra. The equatorial positions are all taken by oxygen. Unlike $Sr_3V_2O_5H_2$, however, the halide ion in these structures is not planar with the alkaline earth metal; it is instead puckered, creating puckered AX_2 layers.

With these structures in mind, we have placed the hydride ion in four different configurations in the Ba1 layer, illustrated in Fig. 3. No configuration was considered where the hydride would replace an oxygen ion or a configuration with random distribution of O^{2-} and H^- at the anionic sites to maintain the non-hydrogen stoichiometry of $Ba_3Ln_2O_5$. Nor was a configuration considered where the hydride was placed within the $Ba_2Ln_2O_5$ layers since this would violate local charge neutrality.

In configurations 1–3, the hydride is in the apical position of the *Ln*-octahedra. In configuration 1, it is planar with Ba1 (similar to the oxyhydride $Sr_3V_2O_5H_2$ [30,31]) in configuration 2, it is placed exactly in

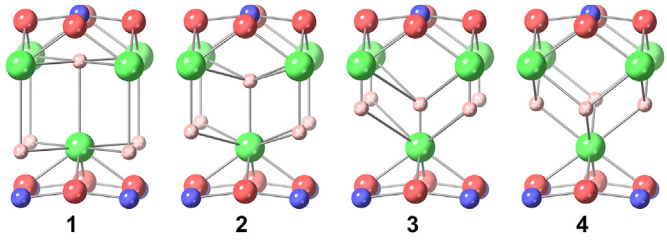

Fig. 3. Four different configurations with H (pink) in the vicinity of Ba1 (green). Blue atoms = *Ln* and red atoms = O.

between *Ln* and Ba1 (similar to the puckered layers in the $Ba_3Bi_2O_5I_2$-type structures [44]), and in configuration 3, it is placed at $z = 1/4$ so that we obtain an H-plane. In configuration 4, the hydride was placed in a tetrahedral position coordinated by four Ba-atoms (still at $z = 1/4$), similar to the Frenkel defect disorder considered in Ln_2LiHO_3 [29]. We calculated the BVS for *Ln* and Ba1 for these configurations. Ba2 is not affected by these hydride locations. The results are summarized in Table 2.

Clearly, configuration 1 is not stable: the BVS for *Ln* are too high, arising from the short *Ln*–H bond (less than 1.9 Å). Likewise, configuration 3 is unphysical: the BVS for Ba1 are over 5, arising from the short Ba1–H bonds (less than 1.8 Å). Configurations 2 and 4, on the other hand, are viable options. In configuration 2, Ba1 in both structures is slightly underbonded (within 0.1) while Lu is slightly overbonded (Yb is near perfect). In configuration 4, Ba1 in both structures is overbonded (by more than 0.2) while Yb is slightly underbonded (Lu is near perfect). Overall, configuration 2 is slightly better overall than configuration 4.

A method to evaluate the stability of a phase is based on DFT calculations, where ground state energies of different structural models can be compared. To shed some light on these two structures (configurations 2 and 4), these were evaluated by DFT. The hydrogen was placed in position (1/2, 1/2, 0.3) for configuration 2 and in position (0, 1/2, 1/4) for configuration 4. We also did consider a structure where the hydride was placed within the $Ba_2Ln_2O_5$ layers but this proved to be ~~so~~ energetically unfavorable and violate local charge neutrality. The structures were optimized, and the relative energies of the optimized structures were calculated to be 0 eV for configuration 2 and 0.87 eV for configuration 4 (and 6.44 eV for the structure with a hydrogen within the $Ba_2Ln_2O_5$ layers).

It is obvious that the structure in configuration 2 – with the hydride ion in one of the apical positions of the *Ln*-centered octahedra – is the more stable one. We therefore consider this structure to be the correct structure of $Ba_3Ln_2O_5H_2$. This is also isostructural to all the other oxyhalides of this structure-type with the halide ions in the same apical position [45–52].

As a further check, an unconstrained refinement of the hydrogen position was carried out. For such a refinement to be successful, it is crucial that the low angle intensities are well determined, and that the anisotropic displacement parameters (ADPs) are well known. Therefore, care was taken to measure a data set with a high number of redundant reflections and extend the angular range (up to $2\theta = 133^\circ$). The latter serves to give well defined atomic positions and ADPs of the heavy atoms. As the form factor of hydrogen contributes to the low angle intensities, an absorption correction based on the measured crystal shape is crucial, and refinement of the secondary extinction coefficient needs to be carried out. With only the Ba, Lu and O positions occupied and fully refined, a difference Fourier map indicated additional electron density consistent with configuration 2. Placing an oxygen atom in this position and refining the occupancy parameter results in a value consistent with a hydrogen atom. This configuration 2 allowed for a constrained refinement of the *z* parameter (fixing the isotropic displacement parameter of hydrogen) that improved the residual agreement factor only by a small amount, indicating that the small form factor of hydrogen is barely affecting the overall agreement. This is not unexpected, since the ratio of number of hydrogen electrons to the overall electron count is of the order of 0.006, thus impressing the need for high redundancy data. The site occupancy of each of the three anionic sites (O1, O2, and H) was checked separately for any indication of mixed-sites, as observed in, e.g., Ba_2ScHO_3 [27]. The site occupancy factor for both O1 and O2 increased slightly, to approximately 1.01, rather than decreasing as would be expected for possible hydrogen admixture. The site occupancy factor for the hydride site decreased to approximately 0.90, rather than increasing and therefore indicating a possible oxygen admixture. We thus conclude that the anions are fully ordered in $Ba_3Ln_2O_5H_2$, and the site occupancy factors were fixed to 1.0. The crystallographic details are summarized in Table 3 and the atomic positions as a result of the refinements are summarized in Table 4. The structure is shown in Fig. 4 along with local atomic environments of Lu and Yb. Fig. 5 shows the local atomic environments of Ba1 and Ba2. Table 5 shows the BVS for these structures.

Table 2
Bond valence sums for *Ln* and Ba1 from the four configurations depicted in Fig. 3.

	$Ba_3Yb_2O_5H_2$		$Ba_3Lu_2O_5H_2$	
	Yb	Ba1	Lu	Ba1
Configuration 1	3.7887	1.7502	3.9242	1.7545
Configuration 2	3.0000	1.9298	3.1045	1.9427
Configuration 3	2.9022	5.2988	3.0036	5.3531
Configuration 4	2.9003	2.2187	3.0016	2.2312

The structure of $Ba_3Ln_2O_5H_2$ is then closely related to the Ruddlesden-Popper (RP) type phase $(ABO_3)_n(AO)$, with $n = 2$. These consist of double layers of ABO_3 perovskite intercalated by single layers of *A*O rock salt. One can consider $Ba_3Ln_2O_5H_2$ to be an $n = 2$ RP phase, albeit with two different anions. $Ba_3Ln_2O_5H_2$ is most closely related to the isostructural series of compounds $Ba_3Ln_2O_5Cl_2$ (*Ln* = Gd–Lu), with the same $Ba_3Ln_2O_5$ perovskite double layer, but with hydrogen in place of chlorine. Similar to $BaCl_2$ in $Ba_3Ln_2O_5Cl_2$, the BaH_2 layer in $Ba_3Ln_2O_5H_2$ between the perovskite layers is of puckered rock salt type. This structural analogy with halides is strongly suggestive of ionic bonding involving H^- anions. The structural motifs present may therefore be written as $Ba_2Ln_2O_5H^{1-} + BaH^{1+}$. Furthermore, the hydrogen atoms ensure local charge neutrality.

The Ln^{3+} ions are octahedrally coordinated by five O-atoms and one H-atom further away, with O2 in the apical position between two *Ln*-atoms and the H-atom in the opposite apical position. The octahedron is distorted with the *Ln*-atom displaced along the *c*-axis off the plane formed by the O1-atoms and towards the O2 atom (see Fig. 4). The atomic environment of Ba1 is a nine-fold coordinated monocapped square antiprismatic polyhedron with four O1-atoms and five H-atoms, while that of Ba2 (located in the perovskite layer) is a 12-fold coordinated cuboctahedron of oxygens (eight O1-atoms and four O2-atoms, typical for the *A* position in perovskite ABO_3 (see Fig. 5). The intercalated slab contains two staggered sheets of BaH with both Ba and H five-coordinated to the other type, similar to the BaCl coordination found in the $Ba_3Ln_2O_5Cl_2$ series of compounds. The BaH layers separate the perovskite slabs, effectively creating a layered system where the intralayer *Ln*–*Ln* distance via the O2-atom is approximately 4.178 Å (*Ln* = Lu) and 4.202 Å (*Ln* = Yb), while the distance between the O1-formed equatorial planes is approximately 6.580 Å (*Ln* = Lu) and 6.584 Å (*Ln* = Yb).

The oxygen atom O2 between the *Ln* ions shows large anisotropic displacement parameters in the *ab*-plane, giving it a pancake-like shape, due to the short *Ln*-O2 bond. This was also observed in $Ba_3Ln_2O_5Cl_2$ and

Table 3
Single crystal x-ray diffraction data and collection parameters for $Ba_3Ln_2O_5H_2$ (*Ln* = Yb, Lu), collected at 180 K and 200 K, respectively.

	$Ba_3Yb_2O_5H_2$	$Ba_3Lu_2O_5H_2$
Molecular weight (g/mol)	840.11 g/mol	843.97 g/mol
Space group	*I*4/*mmm* (#139)	*I*4/*mmm* (#139)
a (Å)	4.3336(2)	4.3291(1)
c (Å)	22.720(1)	22.597(1)
Z	2	2
V (Å^3)	426.67(2)	423.50(1)
ρ_{calc} (g/cm^3)	6.539	6.618
μ (mm^{-1})	35.303	36.795
Data collection range	$3.59^\circ < \theta < 66.22^\circ$	$3.61^\circ < \theta < 66.59^\circ$
Crystal size (mm^3)	0.047 × 0.233 × 0.363	0.010 × 0.072 × 0.084
Reflections collected	9354	22864
Independent reflections	1183	1178
Parameters refined	18	18
R_1, wR_2	0.0579, 0.0647	0.0381, 0.0602
Goodness-of-fit on F^2	0.9999	1.0000

Table 4
Atomic positions of $Ba_3Ln_2O_5H_2$ (Ln = Yb, Lu). The ideal oxygen O2 position has been used (see discussion in the main text).

Atom	Site	x	y	z (Ln = Yb, Lu)	U_{eq} (10^4 Å^2)
Ln	4e	½	½	0.40753(2), 0.40756(2)	68(2), 44(1)
Ba1	4e	0	0	0.32564(3), 0.32583(2)	89(2), 64(2)
Ba2	2b	0	0	½, ½	130(4), 109(2)
O1	8g	0	½	0.3949(4), 0.3956(3)	252(60), 176(30)
O2	2a	½	½	½, ½	359(80), 448(90)
H	4e	½	½	0.3080, 0.2994	200, 200 (U_{iso})

discussed at length [43]: the O2 is displaced from the ideal position. Splitting the O2 atom into four positions did not improve the overall fit to the data, and therefore, the ideal position was retained for the structural figures, although a displacement away from the ideal position increases the *Ln*-O2 distance while decreasing the Ba2–O2 distance, rendering the bond distances more reasonable. Refinements with the O2 atom moved from the ideal position along the [110] direction were stable, indicating a displacement of O2 in the ab-plane of about 0.25 Å and 0.22 Å for Ln = Lu and Yb, respectively. As no superstructure reflections were observed, random or dynamic disorder of oxygen O2 away from the higher symmetry position is therefore assumed. This displacement was of similar magnitude in the $Ba_3Ln_2O_5Cl_2$ series. As seen in Table 1, the BVS indicated severe underbonding of Ba2 in both structures (Ba2 is not affected by the presence of hydrogen in the structure). Reevaluating the BVSs following the same procedure as for the $Ba_3Ln_2O_5Cl_2$ series, viz. using the disordered O2 position, the BVSs of Ba2 improved drastically, increasing from improbable 1.1837 and 1.2253 to reasonable 1.7613 and 1.9439 for the Yb- and Lu-analogs, respectively. These values are similar to the BVSs observed in $Ba_3Yb_2O_5Cl_2$ and $Ba_3Lu_2O_5Cl_2$ [43]. The results are summarized in Table 5. The slight overbonding of the *Ln* BVS is not uncommon and was also observed for the chloride analogs $Ba_3Yb_2O_5Cl_2$ and $Ba_3Lu_2O_5Cl_2$ [43].

Unlike the $Ba_3Ln_2O_5Cl_2$ series, however, the O1 oxygen atoms in $Ba_3Ln_2O_5H_2$ also have large anisotropic displacement parameters; these are cigar-shaped along the *c*-axis and more pronounced for the Yb-analog than for the Lu-analog (see Fig. 4). This, along with the lower Ba2 BVS with displaced O2 in the Yb-analog when compared to the Lu-analog, – 1.7613 vs 1.9439 – hints at the stability limit already at Yb in the lanthanide series for these oxyhydrides. In fact, comparing $Ba_3Ln_2O_5H_2$ to $Ba_3Ln_2O_5Cl_2$, it is apparent that the anion size constrains the formation of possible phases. The larger Cl anion stabilizes the structure for larger *Ln* ions, producing a range from Lu up to Gd. In contrast, for $Ba_3Ln_2O_5H_2$, we observed phase formation for the small lanthanide elements Yb and Lu only. All attempts to synthesize isostructural systems with lanthanides larger than Yb were unsuccessful. We therefore conclude that steric effects limit the size of the lanthanide ion for $Ba_3Ln_2O_5H_2$. Small lanthanides are clearly preferred; while this structure has been observed with Gd and smaller lanthanides for the monovalent X = Cl and with Yb and smaller for monovalent X = H, $Ba_3Yb_2O_5Te$, with a distorted CsCl-type interlayer instead of the BaH layers and with a divalent X = Te, was only found for Yb [41]. This is expected, since perovskite $BaLnO_3$ with lanthanides on the B-site are stable for the smaller lanthanides. While the larger Ba–Cl bonding distance can help stabilizing $Ba_3Gd_2O_5Cl_2$, the considerably shorter Ba–H bonding distance is only sufficient for $Ba_3Yb_2O_5H_2$.

It is interesting to note that the density of states at the valence band edge (see Fig. 6) mostly comprises oxygen 2p orbitals and hydrogen 1s

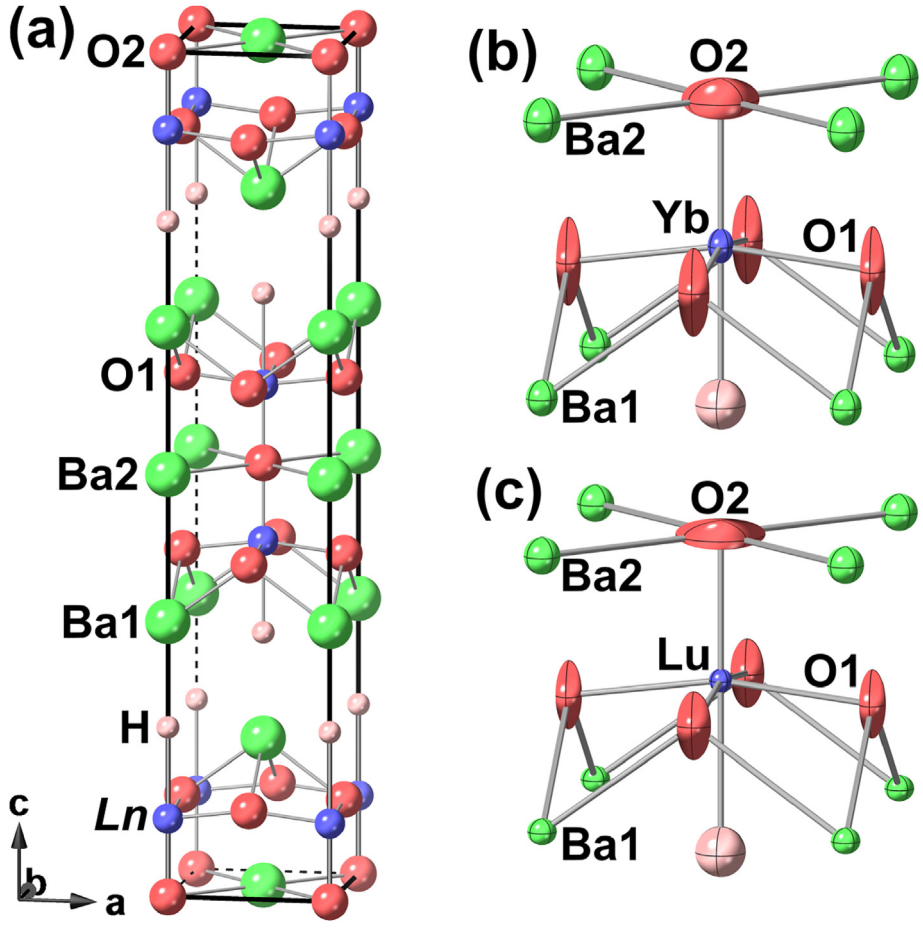

Fig. 4. (a) Unit cell of $Ba_3Ln_2O_5H_2$, along with the octahedrally coordinated local atomic environments of (b) Yb and (c) Lu displaying anisotropic displacement ellipsoids with 95% probability (isotropic for hydrogen).

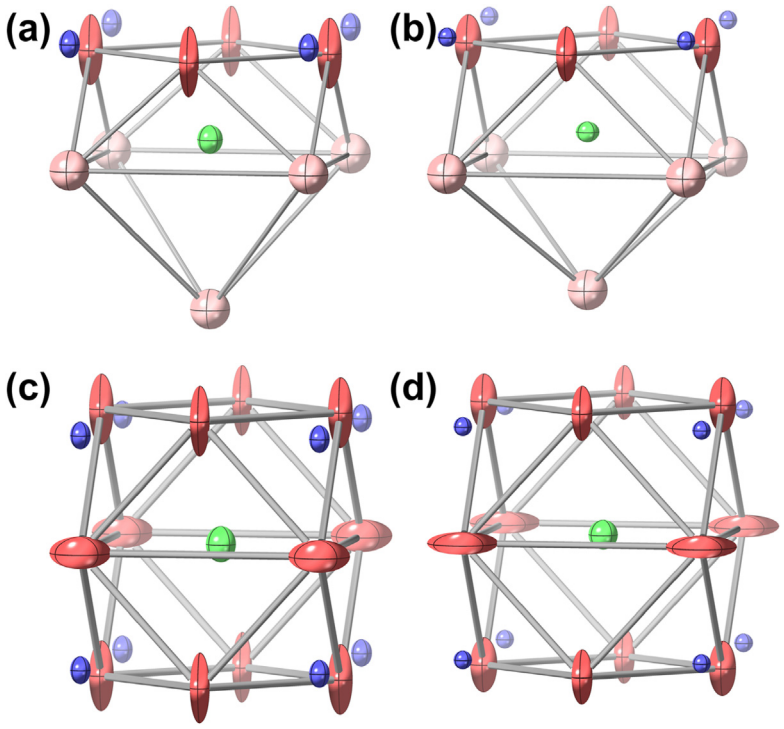

Fig. 5. Atomic environment of Ba1 for (a) $Ba_3Yb_2O_5H_2$ and (b) $Ba_3Lu_2O_5H_2$, and of Ba2 for (c) $Ba_3Yb_2O_5H_2$ and (d) $Ba_3Lu_2O_5H_2$. The "bonds" are drawn to highlight the atomic environments of nine-fold coordinated monocapped square antiprismatic polyhedron for Ba1 and 12-fold coordinated cuboctahedron for Ba2.

Table 5
Bond valence sums for $Ba_3Ln_2O_5H_2$ using both the ideal and the displaced O2 position. The BVS of Ba1 is not affected by the position of O2 and the BVS of Ba2 is not affected by the position of H.

	$Ba_3Yb_2O_5H_2$		$Ba_3Lu_2O_5H_2$	
	Ideal O2 position	Displaced O2	Ideal O2 position	Displaced O2
Ln	3.1973	3.1555	3.1797	3.1231
Ba1	1.7954	1.7954	1.8488	1.8488
Ba2	1.1837	1.7613	1.2253	1.9439

orbitals, in contrast with $Ba_3Lu_2O_5Cl_2$ where the Cl^- anion was not prominent at the valence band edge [43]. This is surprising since the electronegativities of oxygen (3.44) and chlorine (3.16) are closer to each other than those of oxygen and hydrogen (2.2) [6,72]. In the $La_{2-x-y}Sr_{x+y}LiH_{1-x+y}O_{3-y}$ oxyhydrides [10], the valence band edges for the different compounds are dominated by oxygen and hydrogen, while the hydrogen contribution is negligible in $LaSrCoO_3H_{0.7}$ [13,73] and $LaSr_3NiRuO_4H_4$ [32]. The conduction band is formed by barium 5d-orbitals and Lu 5d-orbitals. Anions have spatially extended orbitals and each of the five oxygens has three occupied p orbitals, while each of the two hydrogens has a single s orbital. Both of these factors lead to a lower apparent H weight in the density of states, which nonetheless is well characterized as corresponding to anionic H, similar to anionic H in other compounds [74]. The position of the H 1s states at the top of the valence band in conjunction with its expected chemical flexibility and the observed reactivity of the phases suggests that it may be possible to remove some hydrogen to produce an H deficient material. If so, a Fermi level in the primarily O derived valence band might result. This would be interesting from the point of view of transport and might result in metallic conduction and even superconductivity.

4. Conclusion

Two new oxyhydride phases, $Ba_3Yb_2O_5H_2$ and $Ba_3Lu_2O_5H_2$, were synthesized from molten barium flux with the addition of small amounts of BaH_2. These phases form layered structures isostructural to $Ba_3Bi_2O_5I_2$, with a double perovskite layer containing the lanthanide *Ln* on the perovskite B site. Similar to $Ba_3Ln_2O_5Cl_2$ with puckered BaCl layers, the BaH layers that separate the perovskite layers are also puckered. With barium having a high affinity for hydrogen, a layer type phase is expected, where hydrogen is preferentially located in the vicinity of barium, and oxygen around lanthanides. This begs the question if a corresponding oxyfluoride, with stoichiometry $Ba_3Ln_2O_5F_2$, is possible. The stronger electronegativity of fluorine, however, is expected to change the orbitals at the valence band edge, and may reduce the overall stability. This likely prevented the fluoride analogs of this structure to form despite attempts to synthesize them.

The combination of refinements of data collected via x-ray diffraction, bond valence sum calculations based on the obtained structures, comparisons with other oxyhydrides and oxyhalides, and DFT calculations, the unique position occupied by the anionic hydrogen was unambiguously identified for $Ba_3Ln_2O_5H_2$ (*Ln* = Yb, Lu), and a constrained refinement of the crystallographic data proved stable. We believe that in cases where neutron and NMR/ESR experiments are not feasible, this approach can serve as an alternate way of identifying anionic hydrogen positions in charge compensated systems with distinct anion positions. To our knowledge, this is one of the first studies that uses the combination of structure/synthesis methods and DFT to locate anionic hydrogen in an inorganic compound.

CRediT authorship contribution statement

Tiglet Besara: Data curation, Formal analysis, Investigation, Methodology, Visualization, Writing – original draft, Writing – review & editing. **Daniel C. Ramirez:** Investigation, Writing – original draft. **Jifeng Sun:** Data curation, Formal analysis, Software, Writing – original draft. **Nathaniel W. Falb:** Investigation. **Wangwei Lan:** Investigation, Software. **Jeffrey B. Whalen:** Investigation, Writing – original draft. **David J. Singh:** Formal analysis, Investigation, Resources, Software, Writing – original draft, Writing – review & editing. **Theo Siegrist:**

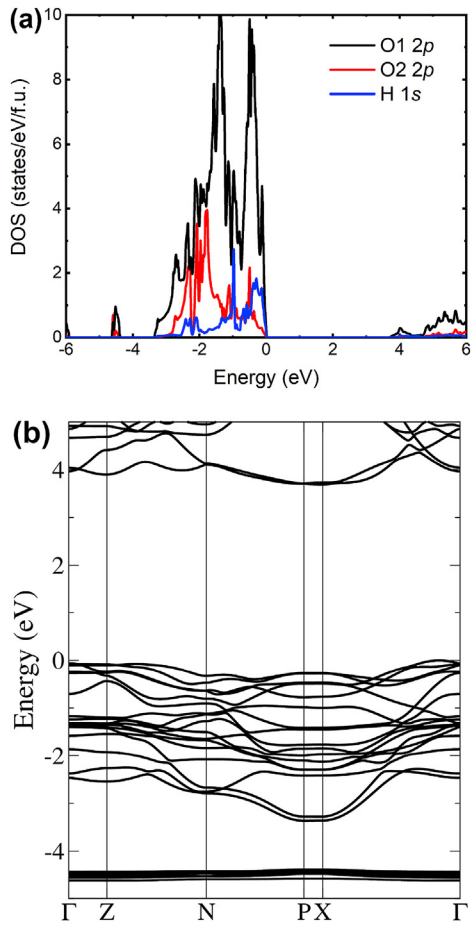

Fig. 6. (a) Projected electronic density of states and (b) band structure of $Ba_3Lu_2O_5H_2$. The flat bands below −4 eV are the upper set of Lu f bands. The valence bands shown are derived from O 2p and H 1s orbitals. The conduction bands have metal character.

Conceptualization, Formal analysis, Funding acquisition, Investigation, Methodology, Resources, Supervision, Writing – original draft, Writing – review & editing.

Declaration of competing interest

The authors declare that they have no known competing financial interests or personal relationships that could have appeared to influence the work reported in this paper.

Data availability

Data will be made available on request.

Acknowledgments

We acknowledge support from the Department of Energy, Basic Energy Sciences, Award DE-SC0008832. Part of the work was carried out at the National High Magnetic Field Laboratory, which is supported by the National Science Foundation, Award DMR 1644779 and the State of Florida. Work at the University of Missouri is supported by the Department of Energy, Basic Energy Sciences, Award DE-SC0019114. We would like to thank Rafael Vasquez and Felix Herrera for helping in the sample synthesis.

References

[1] S.J. Clarke, P. Adamson, S.J.C. Herkelrath, O.J. Rutt, D.R. Parker, M.J. Pitcher, C.F. Smura, Structures, physical properties, and chemistry of layered oxychalcogenides and oxypnictides, Inorg. Chem. 47 (19) (2008) 8473–8486, https://doi.org/10.1021/ic8009964.

[2] D.C. Johnston, The puzzle of high temperature superconductivity in layered iron pnictides and chalcogenides, Adv. Phys. 59 (6) (2010) 803–1061, https://doi.org/10.1080/00018732.2010.513480.

[3] S.D.N. Luu, P. Vaqueiro, Layered oxychalcogenides: structural chemistry and thermoelectric properties, J. Mater. 2 (2) (2016) 131–140, https://doi.org/10.1016/j.jmat.2016.04.002.

[4] L. Zhao, M.T. Fernández-Díaz, L.H. Tjeng, A.C. Komarek, Oxyhalides: a new class of high-T_C multiferroic materials, Sci. Adv. 2 (2016), e1600353, https://doi.org/10.1126/sciadv.1600353.

[5] Y. Kobayashi, O. Hernandez, C. Tassel, H. Kageyama, New chemistry of transition metal oxyhydrides, Sci. Technol. Adv. Mater. 18 (1) (2017) 905–918, https://doi.org/10.1080/14686996.2017.1394776.

[6] H. Kageyama, K. Hayashi, K. Maeda, J.P. Attfield, Z. Hiroi, J.M. Rondinelli, K.R. Poeppelmeier, Expanding frontiers in materials chemistry and physics with multiple anions, Nat. Commun. 9 (1) (2018), https://doi.org/10.1038/s41467-018-02838-4, 772-772.

[7] Y. Kobayashi, Y. Tsujimoto, H. Kageyama, Property engineering in perovskites via modification of anion chemistry, Annu. Rev. Mater. Res. 48 (1) (2018) 303–326, https://doi.org/10.1146/annurev-matsci-070317-124415.

[8] H. Kageyama, T. Yajima, Y. Tsujimoto, T. Yamamoto, C. Tassel, Y. Kobayashi, Exploring structures and properties through anion chemistry, Bull. Chem. Soc. Jpn. 92 (8) (2019) 1349–1357, https://doi.org/10.1246/bcsj.20190095.

[9] M. Udayakantha, P. Schofield, G.R. Waetzig, S. Banerjee, A full palette: crystal chemistry, polymorphism, synthetic strategies, and functional applications of lanthanide oxyhalides, J. Solid State Chem. 270 (2019) 569–592, https://doi.org/10.1016/j.jssc.2018.12.017.

[10] G. Kobayashi, Y. Hinuma, S. Matsuoka, A. Watanabe, M. Iqbal, M. Hirayama, M. Yonemura, T. Kamiyama, I. Tanaka, R. Kanno, Pure H^- conduction in oxyhydrides, Science 351 (6279) (2016) 1314–1317, https://doi.org/10.1126/science.aac9185.

[11] T. Yamamoto, H. Kageyama, Hydride reductions of transition metal oxides, Chem. Lett. 42 (9) (2013) 946–953, https://doi.org/10.1246/cl.130581.

[12] K. Poeppelmeier, A mixed oxide-hydride perovskite, Science 295 (5561) (2002), https://doi.org/10.1126/science.1070030, 1849-1849.

[13] M.A. Hayward, E.J. Cussen, J.B. Claridge, M. Bieringer, M.J. Rosseinsky, C.J. Kiely, S.J. Blundell, I.M. Marshall, F.L. Pratt, The hydride anion in an extended transition metal oxide array: $LaSrCoO_3H_{0.7}$, Science 295 (5561) (2002) 1882–1884, https://doi.org/10.1126/science.1068321.

[14] K. Hayashi, S. Matsuishi, T. Kamiya, M. Hirano, H. Hosono, Light-induced conversion of an insulating refractory oxide into a persistent electronic conductor, Nature 419 (6906) (2002) 462–465, https://doi.org/10.1038/nature01053.

[15] Ø.S. Fjellvåg, Oxyhydrides – Synthesis, Crystal Structure and Properties, Department of Chemistry, University of Oslo, Oslo, Norway, 2019.

[16] C. Eklöf-Österberg, Structure-dynamics Relationships in Perovskite Oxyhydrides and Alkali Silanides, Department of Chemistry and Chemical Engineering, Chalmers University of Technology, Göteborg, Sweden, 2019.

[17] D.F.C. Morris, G.L. Reed, Pauling crystal radius of the hydride ion, J. Inorg. Nucl. Chem. 27 (7) (1965) 1715–1717, https://doi.org/10.1016/0022-1902(65)80037-9.

[18] J.F. Brice, A. Moreau, Synthèse et conductivité anionique des hydruro-oxydes de lanthane de formule LaHO, $LaH_{1+2x}O_{1-x}$ et $LaH_{1+y}O_{1-x}$ ($y < 2x$), Annal. Chim. 7 (1982) 623–634.

[19] B. Huang, J.D. Corbett, Ba_3AlO_4H: synthesis and structure of a new hydrogen-stabilized phase, J. Solid State Chem. 141 (2) (1998) 570–575.

[20] B. Huang, J.D. Corbett, $Ba_{21}Ge_2O_5H_{24}$ and related phases. A corrected structure type and composition for a Zintl phase stabilized by hydrogen, Inorg. Chem. 37 (8) (1998) 1892–1899, https://doi.org/10.1021/ic971339y.

[21] H. Schwarz, Neuartige Hydrid-Oxide der Seltenen Erden: Ln_2LiHO_3 mit Ln = La, Ce, Pr und Nd, Institut für Anorganische Chemie, Karlsruhe Institute of Technology, Karlsruhe, Germany, 1991.

[22] Ø.S. Fjellvåg, J. Armstrong, W.A. Sławiński, A.O. Sjåstad, Thermal and structural aspects of the hydride-conducting oxyhydride La_2LiHO_3 obtained via a halide flux method, Inorg. Chem. 56 (18) (2017) 11123–11128, https://doi.org/10.1021/acs.inorgchem.7b01409.

[23] Ø.S. Fjellvåg, J. Armstrong, P. Vajeeston, A.O. Sjåstad, New insights into hydride bonding, dynamics, and migration in La_2LiHO_3 oxyhydride, J. Phys. Chem. Lett. 9 (2) (2018) 353–358, https://doi.org/10.1021/acs.jpclett.7b03098.

[24] Ø.S. Fjellvåg, K.H. Nygård, P. Vajeeston, A.O. Sjåstad, Advances in the LiCl salt flux method and the preparation of phase pure $La_{2-x}Nd_xLiHO_3$ ($0 \leq x \leq 2$) oxyhydrides, Chem. Commun. 55 (26) (2019) 3817–3820, https://doi.org/10.1039/C9CC00920E.

[25] N. Matsui, G. Kobayashi, K. Suzuki, A. Watanabe, A. Kubota, Y. Iwasaki, M. Yonemura, M. Hirayama, R. Kanno, Ambient pressure synthesis of La_2LiHO_3 as a solid electrolyte for a hydrogen electrochemical cell, J. Am. Ceram. Soc. 102 (6) (2019) 3228–3235, https://doi.org/10.1111/jace.16214.

[26] A. Watanabe, G. Kobayashi, N. Matsui, M. Yonemura, A. Kubota, K. Suzuki, M. Hirayama, R. Kanno, Ambient pressure synthesis and H^- conductivity of $LaSrLiH_2O_2$, Electrochemistry 85 (2) (2017) 88–92, https://doi.org/10.5796/electrochemistry.85.88.

[27] F. Takeiri, A. Watanabe, A. Kuwabara, H. Nawaz, N.I.P. Ayu, M. Yonemura, R. Kanno, G. Kobayashi, Ba_2ScHO_3: H^- conductive layered oxyhydride with H^- site selectivity, Inorg. Chem. 58 (7) (2019) 4431–4436, https://doi.org/10.1021/acs.inorgchem.8b03593.

[28] H. Nawaz, F. Takeiri, A. Kuwabara, M. Yonemura, G. Kobayashi, Synthesis and H^- conductivity of a new oxyhydride Ba_2YHO_3 with anion-ordered rock-salt layers, Chem. Commun. 56 (71) (2020) 10373–10376, https://doi.org/10.1039/D0CC03638B.

[29] Y. Iwasaki, N. Matsui, K. Suzuki, Y. Hinuma, M. Yonemura, G. Kobayashi, M. Hirayama, I. Tanaka, R. Kanno, Synthesis, crystal structure, and ionic conductivity of hydride ion-conducting Ln_2LiHO_3 (Ln = La, Pr, Nd) oxyhydrides, J. Mater. Chem. 6 (46) (2018) 23457–23463, https://doi.org/10.1039/C8TA06880A.

[30] F. Denis Romero, A. Leach, J.S. Möller, F. Foronda, S.J. Blundell, M.A. Hayward, Strontium vanadium oxide-hydrides: "Square-planar" two-electron phases, Angew. Chem. Int. Ed. 53 (29) (2014) 7556–7559, https://doi.org/10.1002/anie.201403536.

[31] T. Yamamoto, H.W.T. Morgan, D. Zeng, T. Kawakami, M. Amano Patino, M.A. Hayward, H. Kageyama, J.E. McGrady, Pressure-Induced transitions in the 1-dimensional vanadium oxyhydrides Sr_2VO_3H and $Sr_3V_2O_5H_2$, and comparison to 2-dimensional $SrVO_2H$, Inorg. Chem. 58 (22) (2019) 15393–15400, https://doi.org/10.1021/acs.inorgchem.9b02459.

[32] L. Jin, M. Lane, D. Zeng, F.K.K. Kirschner, F. Lang, P. Manuel, S.J. Blundell, J.E. McGrady, M.A. Hayward, $LaSr_3NiRuO_4H_4$: a 4d transition-metal oxide-hydride containing metal hydride sheets, Angew. Chem. Int. Ed. 57 (18) (2018) 5025–5028, https://doi.org/10.1002/anie.201800989.

[33] L. Jin, M.A. Hayward, Hole and electron doping of the 4d transition-metal oxyhydride $LaSr_3NiRuO_4H_4$, Angew. Chem. Int. Ed. 59 (5) (2020) 2076–2079, https://doi.org/10.1002/anie.201913951.

[34] L. Jin, M. Batuk, F.K.K. Kirschner, F. Lang, S.J. Blundell, J. Hadermann, M.A. Hayward, Exsolution of SrO during the topochemical conversion of $LaSr_3CoRuO_8$ to the oxyhydride $LaSr_3CoRuO_4H_4$, Inorg. Chem. 58 (21) (2019) 14863–14870, https://doi.org/10.1021/acs.inorgchem.9b02552.

[35] Y. Kobayashi, O.J. Hernandez, T. Sakaguchi, T. Yajima, T. Roisnel, Y. Tsujimoto, M. Morita, Y. Noda, Y. Mogami, A. Kitada, M. Ohkura, S. Hosokawa, Z.F. Li, K. Hayashi, Y. Kusano, J.E. Kim, N. Tsuji, A. Fujiwara, Y. Matsushita, K. Yoshimura, K. Takegoshi, M. Inoue, M. Takano, H. Kageyama, An oxyhydride of $BaTiO_3$ exhibiting hydride exchange and electronic conductivity, Nat. Mater. 11 (6) (2012) 507–511, https://doi.org/10.1038/nmat3302.

[36] T. Sakaguchi, Y. Kobayashi, T. Yajima, M. Ohkura, C. Tassel, F. Takeiri, S. Mitsuoka, H. Ohkubo, T. Yamamoto, J.e. Kim, N. Tsuji, A. Fujihara, Y. Matsushita, J. Hester, M. Avdeev, K. Ohoyama, H. Kageyama, Oxyhydrides of (Ca,Sr,Ba)TiO_3 perovskite solid solutions, Inorg. Chem. 51 (21) (2012) 11371–11376, https://doi.org/10.1021/ic300859n.

[37] H. Yamashita, T. Broux, Y. Kobayashi, F. Takeiri, H. Ubukata, T. Zhu, M.A. Hayward, K. Fujii, M. Yashima, K. Shitara, A. Kuwabara, T. Murakami, H. Kageyama, Chemical pressure-induced anion order-disorder transition in LnHO enabled by hydride size flexibility, J. Am. Chem. Soc. 140 (36) (2018) 11170–11173, https://doi.org/10.1021/jacs.8b06187.

[38] H. Ubukata, T. Broux, F. Takeiri, K. Shitara, H. Yamashita, A. Kuwabara, G. Kobayashi, H. Kageyama, Hydride conductivity in an anion-ordered fluorite structure LnHO with an enlarged bottleneck, Chem. Mater. 31 (18) (2019) 7360–7366, https://doi.org/10.1021/acs.chemmater.9b01968.

[39] B. Malaman, J.F. Brice, Etude structurale de l'hydruro-oxyde LaHO par diffraction des rayons X et par diffraction des neutrons, J. Solid State Chem. 53 (1) (1984) 44–54, https://doi.org/10.1016/0022-4596(84)90226-3.

[40] M. Widerøe, H. Fjellvåg, T. Norby, F. Willy Poulsen, R. Willestofte Berg, NdHO, a novel oxyhydride, J. Solid State Chem. 184 (7) (2011) 1890–1894, https://doi.org/10.1016/j.jssc.2011.05.025.

[41] J.B. Whalen, T. Besara, R. Vasquez, E. Herrera, J. Sun, D. Ramirez, R.L. Stillwell, S.W. Tozer, T.D. Tokumoto, S.A. McGill, J. Allen, M. Davidson, T. Siegrist, A new oxytelluride: perovskite and CsCl intergrowth in $Ba_3Yb_2O_5Te$, J. Solid State Chem. 203 (2013) 204–211, https://doi.org/10.1016/j.jssc.2013.04.030.

[42] T. Besara, M.S. Lundberg, J. Sun, D. Ramirez, L. Dong, J.B. Whalen, R. Vasquez, F. Herrera, J.R. Allen, M.W. Davidson, T. Siegrist, Single crystal synthesis and magnetism of the $BaLn_2O_4$ family (*Ln*= lanthanide), Prog. Solid State Chem. 42 (3) (2014) 23–36, https://doi.org/10.1016/j.progsolidstchem.2014.05.001.

[43] T. Besara, D.C. Ramirez, J. Sun, N.W. Falb, W. Lan, J.N. Neu, J.B. Whalen, D.J. Singh, T. Siegrist, Synthesis and crystal structure of the layered lanthanide oxychlorides $Ba_3Ln_2O_5Cl_2$, Inorg. Chem. 57 (4) (2018) 1727–1734, https://doi.org/10.1021/acs.inorgchem.7b02265.

[44] L.G. Sillén, E. Jörnstad, Einige gemischte wismutoxyjodide, Z. Anorg. Allg. Chem. 250 (2) (1942) 173–198, https://doi.org/10.1002/zaac.19422500206.

[45] R.L. Needs, M.T. Weller, Structure of $Ba_3In_2O_5F_2$ by combined powder X-ray and neutron diffraction analysis; oxide/fluoride ordering in a Ruddlesden-Popper phase, Dalton Trans. 18 (1995) 3015–3017, https://doi.org/10.1039/DT9950003015.

[46] W. Leib, H. Müller-Buschbaum, Ein neues oxohalogenoferrat: $Sr_3Fe_2O_5Cl_2$, Z. Anorg. Allg. Chem. 518 (11) (1984) 115–119, https://doi.org/10.1002/zaac.19845181111.

[47] J.F. Ackerman, The preparation and structures of the alkaline earth iron oxyhalides, J. Solid State Chem. 92 (2) (1991) 496–513, https://doi.org/10.1016/0022-4596(91)90356-M.

[48] F. Letouzé, C. Martin, D. Pelloquin, C. Michel, M. Hervieu, B. Raveau, A thallium oxychloride closely related to the $Sr_3Ti_2O_7$ and $YBaFeCuO_5$ structures: $Ba_3Tl_2O_5Cl_2$, Mater. Res. Bull. 31 (7) (1996) 773–780, https://doi.org/10.1016/0025-5408(96)00065-7.

[49] S.M. Loureiro, C. Felser, Q. Huang, R.J. Cava, Refinement of the crystal structures of strontium cobalt oxychlorides by neutron powder diffraction, Chem. Mater. 12 (10) (2000) 3181–3185, https://doi.org/10.1021/cm000410m.

[50] N. McGlothlin, D. Ho, R.J. Cava, $Sr_3Co_2O_5Cl_2$ and Sr_2CoO_3Cl: two layered cobalt oxychlorides, Mater. Res. Bull. 35 (7) (2000) 1035–1043, https://doi.org/10.1016/S0025-5408(00)00299-3.

[51] C.S. Knee, M.A.L. Field, M.T. Weller, Neutron diffraction study of the antiferromagnetic oxyhalides $Sr_3Fe_2O_5Cl_2$, $Sr_3Fe_2O_5Br_2$ and $Sr_3FeCoO_5Cl_2$, Solid State Sci. 6 (5) (2004) 443–450, https://doi.org/10.1016/j.solidstatesciences.2004.03.002.

[52] M. Abed, H. Müller-Buschbaum, Über ein weiteres Halogeno-Oxoindat $Ba_3In_2O_5Br_2$ mit $Sr_3Ti_2O_7$-Struktur, J. Alloys Compd. 183 (1992) 24–29, https://doi.org/10.1016/0925-8388(92)90727-Q.

[53] Rigaku Oxford Diffraction, CrysAlisPro, 2020. Oxford, UK.

[54] P.W. Betteridge, J.R. Carruthers, R.I. Cooper, K. Prout, D.J. Watkin, CRYSTALS version 12: software for guided crystal structure analysis, J. Appl. Crystallogr. 36 (2003), https://doi.org/10.1107/s0021889803021800, 1487-1487.

[55] L. Palatinus, G. Chapuis, SUPERFLIP - a computer program for the solution of crystal structures by charge flipping in arbitrary dimensions, J. Appl. Crystallogr. 40 (2007) 786–790, https://doi.org/10.1107/s0021889807029238.

[56] C.R. Groom, I.J. Bruno, M.P. Lightfoot, S.C. Ward, The Cambridge structural Database, Acta Crystallogr. B 72 (2) (2016) 171–179, https://doi.org/10.1107/S2052520616003954.

[57] D.J. Singh, L. Nordström, Planewaves, Pseudopotentials and the LAPW Method, second ed., Springer, Berlin, 2006.

[58] K. Schwarz, P. Blaha, G.K.H. Madsen, Electronic structure calculations of solids using the WIEN2k package for material sciences, Comput. Phys. Commun. 147 (1–2) (2002) 71–76, https://doi.org/10.1016/s0010-4655(02)00206-0.

[59] J.P. Perdew, K. Burke, M. Ernzerhof, Generalized gradient approximation made simple, Phys. Rev. Lett. 77 (18) (1996) 3865–3868, https://doi.org/10.1103/PhysRevLett.77.3865.

[60] N.W. Falb, J.N. Neu, T. Besara, J.B. Whalen, D.J. Singh, T. Siegrist, Ba_3CrN_3H: a new nitride-hydride with trigonal planar Cr^{4+}, Inorg. Chem. 58 (5) (2019) 3302–3307, https://doi.org/10.1021/acs.inorgchem.8b03367.

[61] I.D. Brown, The Chemical Bond in Inorganic Chemistry: the Bond Valence Model, Oxford University Press, 2006.

[62] I.D. Brown, Recent developments in the methods and applications of the bond valence model, Chem. Rev. 109 (12) (2009) 6858–6919, https://doi.org/10.1021/cr900053k.

[63] L. Pauling, The principles determining the structure of complex ionic crystals, J. Am. Chem. Soc. 51 (4) (1929) 1010–1026, https://doi.org/10.1021/ja01379a006.

[64] I.D. Brown, Bond valence parameters. https://www.iucr.org/resources/data/data-sets/bond-valence-parameters. (Accessed 15 February 2023).

[65] J.L. Dye, Electrons as anions, Science 301 (5633) (2003) 607–608, https://doi.org/10.1126/science.1088103.

[66] C. Liu, S.A. Nikolaev, W. Ren, L.A. Burton, Electrides: a review, J. Mater. Chem. C 8 (31) (2020) 10551–10567, https://doi.org/10.1039/D0TC01165G.

[67] Y. Zhang, W. Wu, Y. Wang, S.A. Yang, Y. Ma, Pressure-Stabilized semiconducting electrides in alkaline-earth-metal subnitrides, J. Am. Chem. Soc. 139 (39) (2017) 13798–13803, https://doi.org/10.1021/jacs.7b07016.

[68] S. Matsuishi, Y. Toda, M. Miyakawa, K. Hayashi, T. Kamiya, M. Hirano, I. Tanaka, H. Hosono, High-Density Electron Anions in a Nanoporous Single Crystal: $[Ca_{24}Al_{28}O_{64}]^{4+}(4e^-)$, Science 301 (5633) (2003) 626–629, https://doi.org/10.1126/science.1083842.

[69] X. Dong, A.R. Oganov, A.F. Goncharov, E. Stavrou, S. Lobanov, G. Saleh, G.-R. Qian, Q. Zhu, C. Gatti, V.L. Deringer, R. Dronskowski, X.-F. Zhou, V.B. Prakapenka, Z. Konôpková, I.A. Popov, A.I. Boldyrev, H.-T. Wang, A stable compound of helium and sodium at high pressure, Nat. Chem. 9 (5) (2017) 440–445, https://doi.org/10.1038/nchem.2716.

[70] M.-S. Miao, R. Hoffmann, High-pressure electrides: the chemical nature of interstitial quasiatoms, J. Am. Chem. Soc. 137 (10) (2015) 3631–3637, https://doi.org/10.1021/jacs.5b00242.

[71] W. Gutau, H. Müller-Buschbaum, Über ein neues Halogenooxoindat: $Ba_3In_2O_5Cl_2$ mit $Sr_3Ti_2O_7$-Struktur, Z. Anorg. Allg. Chem. 584 (1990) 125–128.

[72] M.W. Cronyn, The proper place for hydrogen in the periodic table, J. Chem. Educ. 80 (8) (2003) 947, https://doi.org/10.1021/ed080p947.

[73] C.A. Bridges, G.R. Darling, M.A. Hayward, M.J. Rosseinsky, Electronic structure, magnetic ordering, and formation pathway of the transition metal oxide hydride $LaSrCoO_3H_{0.7}$, J. Am. Chem. Soc. 127 (16) (2005) 5996–6011, https://doi.org/10.1021/ja042683e.

[74] H. Takenaka, D.J. Singh, Bonding of H in O vacancies of ZnO: density functional calculations, Phys. Rev. B 75 (24) (2007), https://doi.org/10.1103/PhysRevB.75.241102.